Chirality of Topological Gap Solitons in Bosonic Dimer Chains

D. D. Solnyshkov, O. Bleu, B. Teklu, and G. Malpuech
Institut Pascal, PHOTON-N2, University Clermont Auvergne, CNRS, 4 avenue Blaise Pascal, 63178 Aubière Cedex, France
(Received 6 July 2016; published 12 January 2017)

We study gap solitons which appear in the topological gap of 1D bosonic dimer chains within the mean-field approximation. We find that such solitons have a nontrivial texture of the sublattice pseudospin. We reveal their chiral nature by demonstrating the anisotropy of their behavior in the presence of a localized energy potential.

DOI: 10.1103/PhysRevLett.118.023901

Topologically nontrivial structures are currently the focus of attention of the scientific community. Topological insulators are studied in electronic systems for fermionic particles [1] but also in analog systems for bosonic particles (atomic lattices and photonic "topological mirrors" [2–9]). The advantage of artificial photonic systems lies in their design flexibility and the possibility of direct wave function measurements. The properties of such structures are relatively well explored in the linear regime, where the topological invariants have been found to characterize the bands [10] and determine their properties, including the existence of chiral edge states [11] in the gaps. The nonlinear regime is much less explored. Indeed, an interacting quantum fluid exhibits topological properties on its own [12], and one can expect them to become even richer when combined with the linear band topology [13–18].

A one-dimensional (1D) periodic lattice with a certain degree of dimerization is one of the simplest lattices exhibiting topological properties [19–21]. Such a structure shows a splitting of a single *s*-type band into two bands, corresponding to the bonding and antibonding states of the individual dimers. These subbands, characterized by a topological invariant (the Zak phase [22]), are separated by a gap, whose topology is determined by the Zak phase of the band below. The properties of nonlinear solutions existing in this gap can be expected to be strongly affected by its topology. The Su-Schrieffer-Heeger (SSH) soliton is perhaps one of the most famous examples of topologically nontrivial solutions [23] for a dimer chain. However, it involves dynamical dimerization, that is, modification of the properties of the lattice itself: This soliton is a domain wall between two distinct lattices. Similar dimerization domains can be observed in ionic chains [24,25] and artificially created in photonic chains [26]. Recently, chiral solitons of the SSH type were observed in double chains [27]. But there also exist solitonic nonlinear solutions, called gap solitons, that do not require the modification of the lattice and do not close the gap, contrary to the chiral edge states and the SSH soliton. Many of them have been studied in dimerized and zigzag lattices in acoustics [28], Bose condensates [29], and photonic systems [30–33] (including PT-invariant ones [34–38]), with a particularly interesting recent experimental observation [39]. However, the crucial role played by the anisotropy of the Bloch part of the soliton wave function with respect to the two different atoms forming the lattice (and defining the sublattice pseudospin) has remained unnoticed.

In this work, we demonstrate that a gap soliton in a single dimer chain can exhibit chirality. We study a gap soliton in the topological gap of a dimer chain, first using the tight-binding variational approach and then by direct solution of the Gross-Pitaevskii equation with a periodic potential. This solution is strongly different from the SSH soliton [27], because it does not involve the modification of the lattice itself. It is also different from the dark-bright solitons [40], because it does not involve either the polarization degree of freedom or an extended condensate. The topological gap soliton (TGS) is a typical localized solution, appearing from the states at the boundary of a topological gap. We demonstrate that such solitons exhibit a nontrivial pattern of sublattice pseudospin due to pseudospin-anisotropic interactions. We determine their sublattice-polarization degree and demonstrate the chiral nature of these solitons via their asymmetric behavior with respect to a localized defect, which gives a striking contrast with the isotropic behavior of nontopological gap solitons (GSs). These results are confirmed by direct calculations.

The practical realization of the system can be based on a patterned microcavity in the regime of strong coupling [41], with the single-particle states being the cavity exciton polaritons, hybrid light-matter particles characterized by strong interactions thanks to their excitonic fraction, and where bright solitons are observed even without patterning [42,43]. However, our results are valid for any photonic system, where solitonic states can be observed thanks to nonlinearities such as coupled waveguides [26,39], and also for atomic condensates, for which periodic lattices are routinely created [2,44] but which would require putting the condensate out of thermal equilibrium. A closer look at recent experimental data in a photonic dimer chain [39] confirms our predictions for the chiral nature of the TGS.

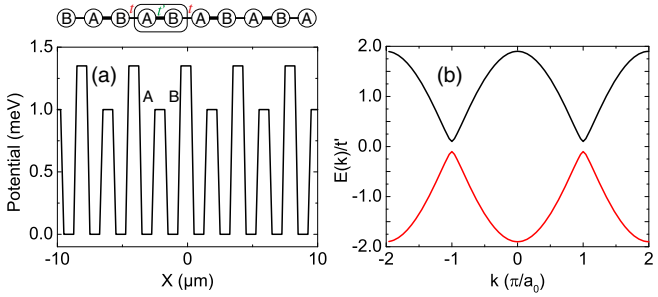

FIG. 1. (a) Periodic potential of a dimer chain and the corresponding tight-binding representation. (b) Tight-binding dispersion of the dimer chain with the topological gap in the middle for $t = 0.9t'$.

Tight-binding description.—A sketch of the dimer chain is shown in Fig. 1(a). Each minimum of the potential corresponds to an individual site, which is called A or B. Since the barriers between the sites have different heights, the tunneling coefficients t and t' are also different. The Hamiltonian can be separated into linear (kinetic) and nonlinear (interaction) parts:

$$\hat{H} = \hat{H}_{\mathrm{lin}} + \hat{H}_{\mathrm{int}}. \tag{1}$$

If one neglects the degree of freedom corresponding to the polarization of light or the spin of electrons, the linear Hamiltonian of a dimer chain can be written as [45]

$$\hat{H}_{\mathrm{lin}} = \sum_m t'\hat{b}_m^\dagger \hat{a}_m + t\hat{a}_{m+1}^\dagger \hat{b}_m + \mathrm{H.c.}, \tag{2}$$

where $\hat{a}, \hat{b}$ are the annihilation operators on the corresponding atoms [A and B, Fig. 1(a)] of the cell m. We assume that $t' > t$, meaning that the unit cell A-B corresponds to a tightly bound "molecule." Using the Bloch theorem, this Hamiltonian can be rewritten in the matrix form in the basis $\psi_k = (\psi_{A,k}, \psi_{B,k})^T$:

$$\hat{H}_{\mathrm{lin}}(k) = -\begin{pmatrix} 0 & t' + te^{-ika_0} \\ t' + te^{ika_0} & 0 \end{pmatrix} \tag{3}$$

with period a_0. The sublattice spinor $(\psi_{A,k}, \psi_{B,k})^T$ allows defining the sublattice pseudospin: $S_Z = (|\psi_A|^2 - |\psi_B|^2)/2$, $S_X = \mathrm{Re}(\psi_A\psi_B^*)$, and $S_Y = \mathrm{Im}(\psi_A^*\psi_B)$. The Hamiltonian can then be represented as an effective magnetic field $\mathbf{\Omega}(k)$ acting on this pseudospin $H = -\hbar\mathbf{\Omega}\mathbf{S}/2$. The dispersion of the chain is plotted in Fig. 1(b). The topological invariant analog, characterizing the two subbands, is the Zak phase [22]. Contrary to the Chern number, the Zak phase is gauge dependent [46]: The unit cell of a chain with inversion symmetry can be chosen for both $t' > t$ and $t' < t$ in such a way [22,47] that the Zak phase of a given band is $\pm\pi$, indicating nontrivial topology (associated with protected edge states in finite chains) induced by the dimerization [48]. The gap between these bands can thus be called "topological."

The nonlinear part of the Hamiltonian reads

$$\hat{H}_{\mathrm{int}} = \frac{\alpha}{2}\sum_m \hat{a}_m^\dagger \hat{a}_m^\dagger \hat{a}_m \hat{a}_m + \hat{b}_m^\dagger \hat{b}_m^\dagger \hat{b}_m \hat{b}_m, \tag{4}$$

where α is the interaction constant. We neglect the interaction between the sites A and B. We then use the mean-field approximation for the macrooccupied state to find the interaction energy.

Variational approach.—The TGS is a stable localized solution of the nonlinear equation, whose energy lies in the topological gap. An ordinary GS with its energy in a semi-infinite gap can also appear in the same lattice. We are going to study the properties of the TGS and compare it with the ordinary GS. To find the nonlinear soliton solution, we use the variational approach. The gap solitons are usually formed from the Bloch states at the edge of the gap. These Bloch states will determine the wave function of the soliton: For TGS, the wave function changes sign between the unit cells ($k = \pi/a_0$), whereas for the ordinary GS (upper gap), the wave function changes sign between each pillar ($k = 2\pi/a_0$). This is why the TGS was also called the antisymmetric soliton [31]. The most important feature of the gap soliton, made of negative mass states, is that it has to maximize the energy and not to minimize it.

In our dimer chain, the trial function has to take into account the fact that the interactions are spin-anisotropic with respect to the sublattice pseudospin. Indeed, a particle on a given site (say, A) interacts only weakly with a particle on a different site (say, B). Maximal interaction energy sought by the soliton is therefore achieved by putting all particles on the same lattice site, that is, by the "circular" polarized states of the sublattice pseudospin, and the corresponding "effective field" is oriented in the Z direction. The pseudospin cannot be constant everywhere, because other terms in the Hamiltonian (appearing due to dimerization) correspond to fields in the X and Y directions (see [48] for details). We can thus expect the soliton pseudospin texture to be nontrivial, as a consequence of the gap topology.

A general shape of the trial function (in the continuous limit) with the two pseudospin components can be constructed using the hyperbolic secant profile, known to be a good solution for the bright soliton of the Gross-Pitaevskii equation:

$$\psi(x, a, b) = 2\sqrt{n/a}\begin{pmatrix} 1/\cosh[(x-b)/a] \\ 1/\cosh[(x+b)/a] \end{pmatrix}, \tag{5}$$

where a is the soliton width, b is the displacement of the maximum of each component with respect to the global center of mass, and n is the soliton density. Close to the edge of the Brillouin zone, the Hamiltonian is reduced to

the Dirac equation with nonlinear terms, extensively studied in the past [29,49–52]. However, it does not have stable solutions in our case because of the pseudospin-anisotropic interactions (see [48] for details). Thus, we consider the full tight-binding Hamiltonian (3) in the reciprocal space and work with the Fourier transforms of the trial wave functions to calculate the kinetic energy $E_{\mathrm{kin}}(a,b)$. To calculate the interaction energy, the integration should be performed in real space:

$$E_{\mathrm{int}}(a) = \frac{1}{2}\alpha \int_{-\infty}^{+\infty} (|\psi_A|^4 + |\psi_B|^4)dx, \tag{6}$$

which gives a $1/a$ dependence $E_{\mathrm{int}} = n^2/12a$.

The variational energy $E_{\mathrm{var}}(a,b) = E_{\mathrm{kin}}(a,b) + E_{\mathrm{int}}(a,b)$ demonstrates a local maximum with respect to both a and b, as shown in Fig. 2(a). The anisotropy of the TGS is clearly visible in this figure: A maximum (marked with a cross) is present only for a positive value of b (determined by the dimerization of the lattice), corresponding to a particular pseudospin texture, whereas the other pseudospin texture does not allow a stable solution (see [48] for details). Therefore, the TGS indeed has a nontrivial pseudospin texture.

Numerical solution.—To verify the analytical solution, we have solved the Gross-Pitaevskii equation for a realistic periodic 1D square potential. The solution on a grid (without the tight-binding approximation) is obtained by using the iterative method. The equation reads

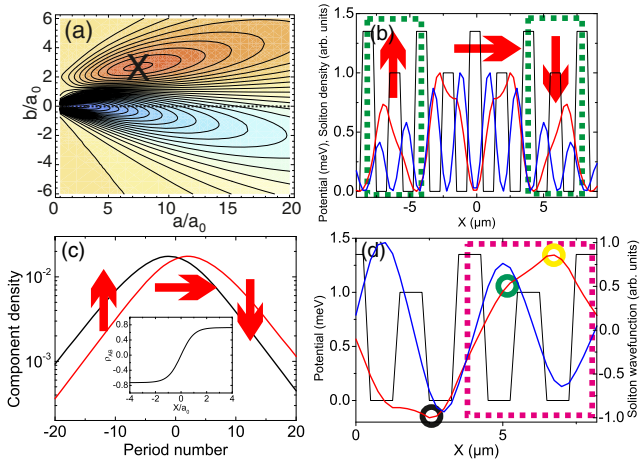

FIG. 2. (a) The energy as a function of variational parameters a, b (red, maximum). (b) Potential profile together with the GS (blue curve) and TGS (red curve) density, demonstrating opposite TGS sublattice polarization (red arrows) on two cells (marked in green). (c) The two sublattice pseudospin components (A, black; B, red) extracted from the full wave function ψ. The inset shows the sublattice polarization degree. (d) Potential and the GS (blue curve) and TGS (red curve) wave functions (circles discussed in the text).

$$E\psi(x) = -\frac{\hbar^2}{2m}\frac{\partial^2}{\partial x^2}\psi(x) + \alpha|\psi(x)|^2\psi(x) + U(x)\psi(x). \tag{7}$$

Here $U(x)$ is the periodic potential of a dimer chain, shown in Fig. 1(a). This equation does not contain the sublattice pseudospin in the explicit way (ψ is not a spinor), because it is not in the tight-binding approximation. However, the pseudospin can be extracted from the solution $\psi(x)$ by analyzing the densities in even and odd minima of the potential separately: $n_{A/B}(x) = \int |\psi(x)|^2 U_{A/B}(x)dx$. Next, we study the internal structure of GS and TGS more in detail to verify our predictions.

Figure 2(b) highlights the two opposite sides of the TGS (red curve), where its sublattice polarization (red arrows) is clearly visible. We see that, counterintuitively, at the left edge the intensity is mostly concentrated on the A atoms ("spin up"), whereas on the right edge the intensity is on the B atoms ("spin down"), contrary to the GS (blue curve), showing a typical soliton profile. This feature is present in calculated and measured figures of Refs. [31,32,39], but it has not drawn the attention it deserves as a signature of anisotropy of the soliton. The extracted density of each sublattice pseudospin component (black and red curves) is shown in Fig. 2(c). The log scale plot clearly exhibits a $1/\cosh^2(x/a)$ dependence of a bright soliton, with the two components displaced with respect to the soliton center, justifying our trial wave function.

Analysis of the TGS features.—The variational approach allows us to find the sublattice-polarization degree ρ_{AB} of the TGS, which is the density difference between the A and B sites [see the inset in Fig. 2(c)],

$$\rho_{AB}(x) = \tanh(b/a)\tanh(x/a), \tag{8}$$

which, considering the limit $x \to \infty$, gives $\rho_{AB\infty} = \tanh b/a$. This result characterizes the sublattice-polarization texture of the gap soliton, and, since the soliton size a decreases with the number of particles while b remains fixed, its polarization degree increases with n.

The counterintuitive TGS density distribution within the unit cell, with more particles on the pillar away from the soliton center (contrary to the usual GS), can be understood qualitatively from Fig. 2(d), showing the wave function over two unit cells. To maximize the interaction energy, the particle distribution within each dimer (rose rectangle) should be maximally anisotropic, and the particles tend to localize on either A (green circle) or B (yellow circle). On the other hand, the main contribution to the kinetic energy is due to the change of sign of the wave function between the cells. Its minimization imposes the wave function to be minimal on the A pillar (green circle), because the neighboring cell is closer to the TGS center and thus has a higher density (black circle) than the other neighbor. This is in contrast with the ordinary GS, which has a wave function

changing sign between *each* pillar and is therefore not subject to this polarization mechanism.

The opposite polarization degree of the sublattice pseudospin on each side is crucial, because it distinguishes the TGS from the GS of the upper gap and leads to the anisotropic behavior of the TGS. It can be experimentally probed by considering the effect of a localized potential breaking the symmetry between the A and B sites. In the tight-binding approximation, such potential can be expressed as a local effective magnetic field $\Omega_Z = \delta(x)$, and the energy of the soliton centered at x_0 in the presence of such a field is given by

$$E_{\mathrm{TGS}} = \int \Omega \cdot \mathbf{S} dx \propto \frac{\tanh(b/a)\tanh(x_0/a)}{\cosh^2(x_0/a)}. \quad (9)$$

The asymmetry of this expression is seen in Fig. 3(a) (gray line). A TGS located on one side of the field will be attracted to the defect, whereas a TGS located on the other side will be repelled to infinity as indicated by the black arrows. On the contrary, the energy of the ordinary GS formed from the states of the upper band in the presence of a δ potential can be written as

$$E_{\mathrm{GS}} = \int V(x)|\psi(x)|^2 dx \propto \frac{1}{\cosh^2(x_0/a)}. \quad (10)$$

It is plotted in Fig. 3(a) (blue line): A positive localized potential attracts the ordinary GS whatever its initial position, which oscillates around this defect.

Chiral dynamics.—We have calculated the dynamics of both TGS and GS solving Hamilton's equations:

$$\dot{x}_0 = \frac{\partial H}{\partial p_0}, \qquad \dot{p}_0 = -\frac{\partial H}{\partial x_0}, \quad (11)$$

where x_0 and p_0 are the TGS or GS position and momentum, respectively, and its Hamiltonian is

$$H(x_0, p_0) = \frac{p_0^2}{2m} + E_{\mathrm{TGS/GS}}(x_0), \quad (12)$$

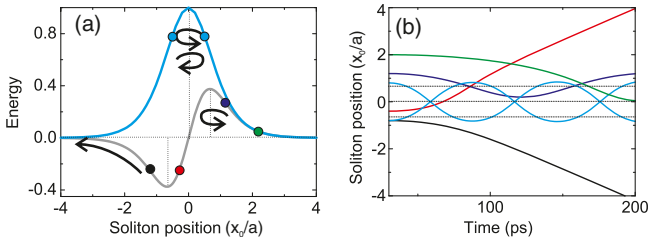

FIG. 3. (a) Energy of the soliton as a function of its position with respect to the localized potential $\delta(x)$: TGS (gray curve) and GS (blue curve). (b) Soliton trajectories of different families: TGS (black, red, navy, and green curves) and GS (cyan curve).

where m is the soliton mass. We take $p_0(t=0) = 0$ as an initial condition. The resulting soliton trajectories can be classified into several families, depending on the initial position $x_0(t=0)$ and on the soliton type, shown in Fig. 3(b). The ordinary GS trajectories are shown in cyan, for the initial positions shown as cyan points in Fig. 3(a). The GS is always confined and exhibits anharmonic oscillations because of the potential profile $E_{\mathrm{GS}} \propto 1/\cosh^2(x_0/a)$. The TGS can be either confined [blue and green lines, initial positions in blue and green in Fig. 3(a)] or delocalized (black and red curves). The regime depends on the sign of the TGS energy determined by its initial position $x_0(t=0)$. The period of the anharmonic oscillations for the localized case strongly depends on the energy (compare blue and green curves).

This behavior, which is the main dynamical consequence of the TGS chirality, is confirmed by numerical simulations, shown in Fig. 4, performed by solving the time-dependent Gross-Pitaevskii equation

$$i\hbar \frac{\partial \psi}{\partial t} = -\frac{\hbar^2}{2m}\Delta\psi + \alpha|\psi|^2\psi + U\psi \quad (13)$$

for polaritons (see [48]) with a pulsed excitation

$$\psi(x)|_{t=0} = \sqrt{n} e^{-(x-x_0)^2/\sigma^2} \sin\left(\frac{2\pi x}{a_0}\right) \cos\left(\frac{\pi x}{a_0}\right) \quad (14)$$

for TGS and without the cosine for GS. Depending on the initial position, the TGS is either attracted to the pointlike magnetic field, in which case it oscillates [Fig. 4(a)], or

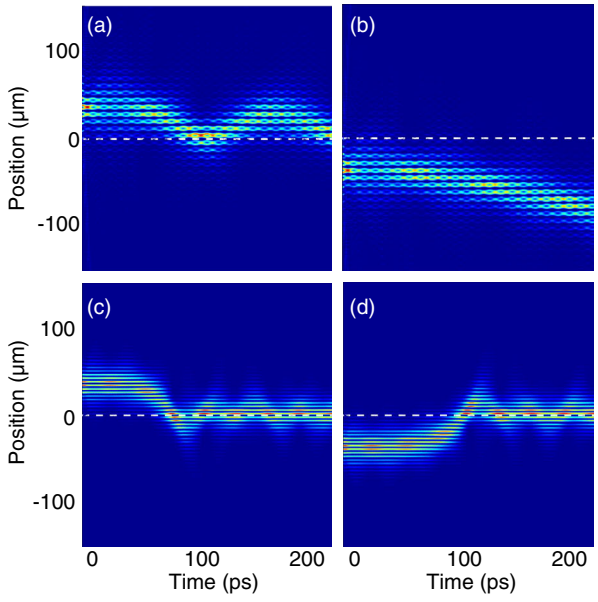

FIG. 4. Soliton trajectories plotted as the particle density as a function of position and time: (a),(b) TGS, oscillating trajectory, or free acceleration, depending on the initial soliton position. (c), (d) Oscillating trajectory of an ordinary GS for the same defect.

repelled and accelerated away from it [Fig. 4(b)]. This behavior is a clear signature of its anisotropy, manifested in the pseudospin pattern. Contrary to the TGS, an ordinary GS does not exhibit this anisotropic behavior [oscillating behavior in both Figs. 4(c) and 4(d)], because it does not have the chiral pseudospin texture. The agreement between the analytical model based on the Hamilton's equations and the full numerical simulations can be seen in Supplemental Material ([48], Fig. S2).

In conclusion, we have analyzed the properties of solitons in the topological gap of a 1D bosonic dimer chain. We have found that such solitons exhibit a chiral pattern of their sublattice pseudospin, allowing them to behave anisotropically, contrary to the ordinary GS. The soliton wave function and the resulting pseudospin texture are obtained analytically in the tight-binding approximation using a variational approach. These results are confirmed by the direct numerical solution of the GP equation and are by several aspects comparable with those of previous theoretical works [31,32] and with a recent experimental observation [Fig. 2(b) of Ref. [39]]. However, the crucial anisotropic pseudospin texture and the chiral behavior of the antisymmetric soliton have passed unnoticed in these works.

We acknowledge the support of the project "Quantum Fluids of Light" (ANR-16-CE30-0021).

[1] M. Z. Hasan and C. L. Kane, Rev. Mod. Phys. **82**, 3045 (2010).
[2] I. I. Satija and E. Zhao, in *New Trends in Atomic and Molecular Physics*, edited by M. Mohan (Springer-Verlag, Berlin, 2013), Chap. 12, p. 201.
[3] M. Aidelsburger, M. Lohse, C. Schweizer, M. Atala, J. T. Barreiro, S. Nascimbene, N. Cooper, I. Bloch, and N. Goldman, Nat. Phys. **11**, 162 (2015).
[4] H. Schomerus, Opt. Lett. **38**, 1912 (2013).
[5] L. Lu, J. Joannopoulos, and M. Soljacic, Nat. Photonics **8**, 821 (2014).
[6] A. Poddubny, A. Miroshnichenko, A. Slobozhanyuk, and Y. Kivshar, ACS Photonics **1**, 101 (2014).
[7] A. V. Poshakinskiy, A. N. Poddubny, and M. Hafezi, Phys. Rev. A **91**, 043830 (2015).
[8] A. P. Slobozhanyuk, A. N. Poddubny, A. E. Miroshnichenko, P. A. Belov, and Y. S. Kivshar, Phys. Rev. Lett. **114**, 123901 (2015).
[9] I. S. Sinev, I. S. Mukhin, A. P. Slobozhanyuk, A. N. Poddubny, A. E. Miroshnichenko, A. K. Samusev, and Y. S. Kivshar, Nanoscale **7**, 11904 (2015).
[10] B. Simon, Phys. Rev. Lett. **51**, 2167 (1983).
[11] Y. Hatsugai, Phys. Rev. Lett. **71**, 3697 (1993).
[12] G. Volovik, *The Universe in a Helium Droplet* (Clarendon, Oxford, 2003).
[13] Y. Lumer, Y. Plotnik, M. C. Rechtsman, and M. Segev, Phys. Rev. Lett. **111**, 243905 (2013).
[14] S. Furukawa and M. Ueda, New J. Phys. **17**, 115014 (2015).
[15] G. Engelhardt and T. Brandes, Phys. Rev. A **91**, 053621 (2015).
[16] O. Bleu, D. D. Solnyshkov, and G. Malpuech, Phys. Rev. B **93**, 085438 (2016).
[17] Z.-F. Xu, L. You, A. Hemmerich, and W. V. Liu, Phys. Rev. Lett. **117**, 085301 (2016).
[18] M. Di Liberto, A. Hemmerich, and C. M. Smith, Phys. Rev. Lett. **117**, 163001 (2016).
[19] S. Ryu, A. P. Schnyder, A. Furusaki, and A. W. W. Ludwig, New J. Phys. **12**, 065010 (2010).
[20] J. K. Asboth, L. Oroszlany, and A. Palyi, *A Short Course on Topological Insulators* (Springer International, New York, 2016).
[21] H.-M. Guo, Sci. China Phys. Mech. Astron. **59**, 637401 (2016).
[22] J. Zak, Phys. Rev. Lett. **62**, 2747 (1989).
[23] W. P. Su, J. R. Schrieffer, and A. J. Heeger, Phys. Rev. B **22**, 2099 (1980).
[24] A. del Campo, G. De Chiara, G. Morigi, M. B. Plenio, and A. Retzker, Phys. Rev. Lett. **105**, 075701 (2010).
[25] K. Pyka *et al.*, Nat. Commun. **4**, 2291 (2013).
[26] A. Blanco-Redondo, I. Andonegui, M. J. Collins, G. Harari, Y. Lumer, M. C. Rechtsman, B. J. Eggleton, and M. Segev, Phys. Rev. Lett. **116**, 163901 (2016).
[27] S. Cheon, T.-H. Kim, S.-H. Lee, and H. W. Yeom, Science **350**, 182 (2015).
[28] Y. S. Kivshar and N. Flytzanis, Phys. Rev. A **46**, 7972 (1992).
[29] L. H. Haddad, C. M. Weaver, and L. D. Carr, New J. Phys. **17**, 063033 (2015).
[30] A. A. Sukhorukov and Y. S. Kivshar, Opt. Lett. **27**, 2112 (2002).
[31] N. K. Efremidis and D. N. Christodoulides, Phys. Rev. E **65**, 056607 (2002).
[32] R. A. Vicencio and M. Johansson, Phys. Rev. A **79**, 065801 (2009).
[33] S. V. Dmitriev, A. A. Sukhorukov, and Y. S. Kivshar, Opt. Lett. **35**, 2976 (2010).
[34] Z. H. Musslimani, K. G. Makris, R. El-Ganainy, and D. N. Christodoulides, Phys. Rev. Lett. **100**, 030402 (2008).
[35] S. V. Suchkov, B. A. Malomed, S. V. Dmitriev, and Y. S. Kivshar, Phys. Rev. E **84**, 046609 (2011).
[36] P. P. Beličev, I. Ilić, A. Maluckov, M. Stepić, A. Kanshu, C. E. Rüter, and D. Kip, Phys. Rev. A **86**, 033835 (2012).
[37] M. Wimmer, A. Regensburger, M.-A. Miri, C. Brtdvh, D. Christodoulides, and U. Peschel, Nat. Commun. **6**, 7782 (2015).
[38] S. V. Suchkov, A. A. Sukhorukov, J. Huang, S. V. Dmitriev, C. Lee, and Y. S. Kivshar, Laser Photonics Rev. **10**, 177 (2016).
[39] A. Kanshu, C. E. Ruter, D. Kip, V. Shandarov, P. P. Pelicev, I. Ilic, and M. Stepic, Opt. Lett. **37**, 1253 (2012).
[40] D. D. Solnyshkov, A. V. Nalitov, and G. Malpuech, Phys. Rev. Lett. **116**, 046402 (2016).
[41] D. Tanese *et al.*, Nat. Commun. **4**, 1749 (2013).
[42] O. A. Egorov, D. V. Skryabin, A. V. Yulin, and F. Lederer, Phys. Rev. Lett. **102**, 153904 (2009).
[43] M. Sich, D. N. Krizhanovskii, M. S. Skolnick, A. V. Gorbach, R. Hartley, D. V. Skryabin, E. A. Cerda-Mendez, K. Biermann, R. Hey, and P. V. Santos, Nat. Photonics **6**, 50 (2012).

[44] L. Pitaevskii and S. Stringari, *Bose-Einstein Condensation*, International Series of Monographs on Physics Vol. 116 (Oxford Science, New York, 2003).
[45] P. Delplace, D. Ullmo, and G. Montambaux, Phys. Rev. B **84**, 195452 (2011).
[46] M. Atala, M. Aidelsburger, J. T. Barreiro, D. Abanin, T. Kitagawa, E. Demler, and I. Bloch, Nat. Phys. **9**, 795 (2013).
[47] W. Kohn, Phys. Rev. **115**, 809 (1959).
[48] See Supplemental Material at http://link.aps.org/supplemental/10.1103/PhysRevLett.118.023901 for extra results of numerical simulations.
[49] J. Werle, Phys. Lett. **71B**, 357 (1977).
[50] K. Takahashi, J. Math. Phys. (N.Y.) **20**, 1232 (1979).
[51] T. Bartsch and Y. Ding, J. Differ. Equations **226**, 210 (2006).
[52] D. E. Pelinovsky and A. Stefanov, J. Math. Phys. (N.Y.) **53**, 073705 (2012).